AIAA JOURNAL
Vol. 40, No. 9, September 2002

Forward Flight Stability Characteristics for Composite Hingeless Rotors with Transverse Shear Deformation

Sung Nam Jung*
Chonbuk National University, Chonju 561-756, Republic of Korea
and
Kyung Nam Kim† and Seung Jo Kim‡
Seoul National University, Seoul 151-742, Republic of Korea

The shaft-fixed aeroelastic stability behavior of a soft-in-plane, composite hingeless rotor blade in hover and in forward flight has been investigated by using the finite element method in both space and time. The nonclassical structural effects, such as anisotropy, transverse shear, and torsion warping, are incorporated in the structural formulation. Timoshenko-type shear correction coefficients, which take into account the bending–shear and extension–shear couplings, are introduced to consider the nonuniform distribution of shear across the section of the blade. The aerodynamic model in the current aeroelastic analysis is formulated to allow either quasi-steady or unsteady two-dimensional aerodynamics. The Leishman–Beddoes model based on an indicial response method is employed to consider the unsteady aerodynamic effects. The effects of compressibility and reversed flow are also incorporated. Finite element equations of motion undergoing moderately large displacements and rotations are derived using the Hamilton's principle. Numerical simulations are carried out to validate the current analysis with other literature. The influence of composite couplings, transverse shear deformation, and unsteady aerodynamics on the aeroelastic behavior of soft-in-plane helicopter blades is investigated. Numerical results illustrating a great potential to improve the aeroelastic stability are presented for a blade with positive tension–pitch coupling. The transverse shear deformation is seen to have a stabilizing effect on the lag mode stability for cases with elastic couplings. Overall, the transverse shear effects become larger at higher forward speeds. It is also seen that the lag mode stability is significantly influenced by the unsteady aerodynamic effects.

Nomenclature

A	=	cross-sectional area
C_T	=	rotor thrust coefficient
c	=	blade chord
R	=	blade length
u, v, w, ϕ	=	elastic beam deflections
X, Y, Z	=	hub-fixed rotating coordinates
X_H, Y_H, Z_H	=	hub-fixed nonrotating coordinates
x, y, z	=	undeformed blade coordinates
α_ζ	=	lag mode damping, per revolution
β_p	=	precone angle
$\varepsilon_{xx}, \gamma_{x\eta}, \gamma_{x\zeta}$	=	engineering strains
θ_{tw}	=	blade pretwist angle
θ_0	=	blade pitch, $\theta_{0.75} + \theta_{\text{tw}}(x/R - 0.75) + \theta_{1c}\cos\psi + \theta_{1s}\sin\psi$
$\theta_{0.75}$	=	collective pitch at 75% radius
θ_{1c}, θ_{1s}	=	cyclic pitch
$\bar{\theta}$	=	total blade pitch, $\theta_0 + \phi$
μ	=	advance ratio
ξ, η, ζ	=	deformed beam coordinates
ρ	=	mass density
σ	=	solidity ratio
$\sigma_{xx}, \tau_{x\eta}, \tau_{x\zeta}$	=	engineering stresses
ψ	=	azimuth angle, Ωt
Ω	=	rotor speed, rpm

Superscripts

$'$	=	$\mathrm{d}(\ )/\mathrm{d}x$
$\cdot$	=	$\mathrm{d}(\ )/\mathrm{d}t$

Received 23 August 2001; revision received 14 March 2002; accepted for publication 16 April 2002.

*Associate Professor, Department of Aerospace Engineering. Member AIAA.
†Graduate Research Assistant, School of Mechanical and Aerospace Engineering; currently Research Engineer, Korea Institute of Aerospace Technology, Korean Air, Daejon 305-811, Republic of Korea.
‡Professor, School of Mechanical and Aerospace Engineering. Member AIAA.

Introduction

THE aeroelastic stability analysis of composite rotor blades has generally been performed through the one-dimensional beam assumption, given that the longitudinal dimension of the blade is much larger compared to the lateral ones.[1] This rather intuitive assumption has been validated by considering relative strain energies between the real and the idealized structures from a three-dimensional elasticity point of view.[2,3] Many simplifying assumptions may be drawn for the beam kinematics, but it is important to capture appropriately nonclassical structural effects such as transverse shear, warping, and warping restraint for accurate analysis results. To describe these nonclassical effects in the analysis of a composite blade, published works have used two distinct approaches. The first class includes cross-sectional finite element analysis, such as VABS,[3] that can model complex geometry and nonuniformity of a cross section in a straightforward way. The second class includes analytical models such as those of Rehfield[4] and Smith and Chopra[5] that are simple and can be used to provide physical insights into the relationship between the various effects. Although finite element models can be very useful in the detailed design stage of composite rotors, the analytical models seem to be extremely useful in the preliminary design stage, including optimization studies and aeroelastic stability analyses.[6]

During the past two decades, there has been remarkable research activity into the aeroelastic stability analysis of composite rotor blades. Existing aeroelastic analyses can be divided into two types, based on the treatment of geometric nonlinearities retained in the one-dimensional beam representation. The first type is based on a moderate deflection beam theory, where an ordering scheme is introduced to discard small, higher-order nonlinear terms that arise in

the derivation of motion equations. Typically, the bending deflections are assumed to be of order ε, and terms up to order ε^2 or order ε^3 are retained in the analysis. In the second type, large deflection beam theory that removed the restrictions on the magnitude of the deformations is used. Fulton and Hodges[7] and Shang et al.[8] studied the stability behavior of composite hingeless rotors in hovering flight. The analyses placed no restrictions on the magnitude of deformations of the blade. These studies showed that the discrepancy between numerical and experimental results for lag mode damping of the small-scale rotor of Sharpe[9] was not caused by modeling errors associated with large deflections of the beam. Even though there remains some debate on the treatment of the geometric nonlinearities of rotors, this study gives one the idea that the first type of approach actually leads to an accuracy of solutions comparable to the second type in the aeroelastic analysis. Note that the first type of analysis is commonly used for metallic blades and has also been used for composite blades by a number of researchers (for example, see Ref. 10), the present paper included.

Hong and Chopra[11] used a moderate deflection type of beam theory to examine the effects of elastic couplings of composite rotors on the aeroelastic stability in hover. Some of the important nonclassical effects, such as transverse shear couplings, were ignored in the analysis, but the study showed a potential to improve the aeroelastic stability by tailoring the composite couplings of the blade. Panda and Chopra[12] extended this research to include dynamics of composite rotors in forward flight. This work showed the possibility of reducing stress and vibration levels using composite tailoring techniques. Yuan et al.[13] presented a finite element based aeroelastic stability analysis for single- and double-celled composite hingeless rotors with straight and swept tips in hovering flight. Moderate deflection and finite rotation assumptions were used in the analysis. In the finite element model, kinematic variables associated with transverse shear and torsion warping were included as separate degrees of freedom (DOF) that result in 23 DOF per element. They concluded that geometric design parameters, such as blade sweep, as well as composite couplings, can be exploited in the structural design studies.

Smith and Chopra[14] studied the aeroelastic behavior of elastically coupled composite hingeless rotors in forward flight. A shear flexible 19-DOF beam finite element, including four transverse shear DOF was developed for the analysis. Several blade configurations that represent pitch–flap, pitch–lag, and tension–pitch couplings were considered to investigate the influence of composite couplings on the aeroelastic stability response of the rotors. The study presented the great potential of using composite couplings but, among others, demonstrated the possibility that negative pitch–lag couplings (lag back/pitch up deformation) could be very effective in controlling the aeroelastic stability boundary. In this study, however, the distribution of shear was assumed (implicitly) as uniform across the section of the blade. Tracy and Chopra[15] investigated the aeroelastic stability of a soft-in-plane bearingless rotor in forward flight. In this analysis, the flexbeam was modeled as a composite thin-walled I beam, whereas the main blade and torque tube were idealized as thin-walled closed box-section beam. Transverse shear effects were included implicitly by statically condensing the shear DOF in the finite element model. The effects of composite couplings were seen to have a significant effect on the stability behavior of composite bearingless rotors.

Jung and Kim[16,17] investigated the effects of transverse shear deformation and structural damping on the aeroelastic response of stiff-in-plane composite hingeless rotors in hover. The study introduced shear correction factors (SCF) to account for the nonuniform distribution of shear across the section and presented improved results (3–15%) over those of Smith and Chopra[14] for the structural dynamics analysis of rotating composite box-beams. Note that Smith and Chopra used a Timoshenko-type theory with the shear correction factor set to unity. Jung and Kim's studies[16,17] showed that the effects of transverse shear and structural damping can have a key role in the prediction of the flutter boundary of the rotor but that the flight envelope was confined to hovering flight and that the SCF used was obtained from the formula[18] of an isotropic thin-walled box section. Kim et al.[19] studied the shear stress distribution across both rectangular solid and thin-walled box sections and obtained the formula of SCF in closed form by using the equivalence of strain energy between the real cross section and a section subjected to the same shear force, but with an effective area over which the shear stress is uniform. The effects of elastic couplings, as well as the geometry, of a section were taken into account to determine the SCF.

During the past few decades, many studies have been focused on showing the importance of including the transverse shear deformation on the static,[6,20] structural dynamic,[14,16] and hover aeroelastic stability analyses[16,17] of composite blades. The influence of transverse shear deformation can be included in a beam formulation in an explicit[13,14,16] or implicit[15] manner. The implicit method has a certain advantage over the explicit one in that no additional DOF are required in carrying out the computation. However, as pointed out by Jung et al.,[6] the accuracy of the solution via the implicit method may be questionable even for a short, slender composite beam, especially when the beam is under the action of two perpendicular loads with different magnitudes, which is very similar to the case of a helicopter blade where the aerodynamic forces acting in the flatwise direction are much larger than those in the chordwise direction. Note that, in Ref. 6, only the static case was considered to investigate the effect of transverse shear on the beam response. So far, the direct effects of transverse shear deformation on the aeroelastic stability of composite rotors in forward flight have not been exploited in the literature. Furthermore, despite the evident practical importance of the field, the published works devoted to the aeromechanical instability of a composite rotor blade (especially in forward flight) that includes the unsteady aerodynamic effects are still rare.[6]

In the present work, the aeroelastic stability (shaft-fixed) behavior of composite hingeless rotor blades in forward flight is investigated by using the finite element method. The blade structure is idealized as a thin-walled, single-celled box-section beam. The structural model is based on the work of Jung and Kim,[16] who take into account key nonclassical structural effects such as anisotropy, transverse shear, and torsion warping. For this study, the wall of the box section is assumed as the membrane. The level of approximation used in the beam kinematics corresponds to Timoshenko for bending and to St. Venant for torsion. The warping restraint effect is neglected in the analysis. A newly derived formula of SCF[19] that is a function of composite couplings, as well as the geometry of the section, is used to take into account the nonuniform distribution of shear over the section of the blade. Special focus is given to identify the effects of transverse shear deformation on the stability boundary of the blade. Either quasi-steady or unsteady two-dimensional aerodynamics is employed to study the unsteady aerodynamic effects on the stability behavior of the blade. The aerodynamic model developed by Leishman and Beddoes[21] is adopted for the unsteady aerodynamics. This model is based on an indicial response method and is valid for attached flow, separated flow, and dynamically stalled flow. Compressibility and reversed flow effects are also incorporated in the present analysis.

Recently, more generic beam models such as those of Volovoi and Hodges[22] and Jung et al.[23] have been developed. These beam theories allow treatment of arbitrary cross-sectional geometries and material distributions. The bending strain measures, as well as the membrane strains, were included in these formulations to take into account the wall thickness effect of the beam cross section. Note that a more rigorous representation of beam kinematics is truly desirable for accurate analysis, but a comprehensive aeroelastic analysis of composite rotors (especially in forward flight) with these state-of-the-art beam models has not been reported yet. Also, there is a need to fill the apparent existing gap in the literature, and this work aims at providing the relevant information in the related field.

Note that, to the best of the authors' knowledge, the present work is the first to investigate the direct transverse shear effects on the aeroelastic stability of coupled composite blades in forward flight. Results illustrating a great potential for the aeroelastic tailoring are also presented for composite blades with tension–pitch couplings, which have received less attention compared to the pitch–flap, δ_3, or pitch–lag, α_1, types of elastic couplings. In addition, the effects of unsteady aerodynamics on the stability boundary of composite hingeless rotors are examined in the framework of the analysis.

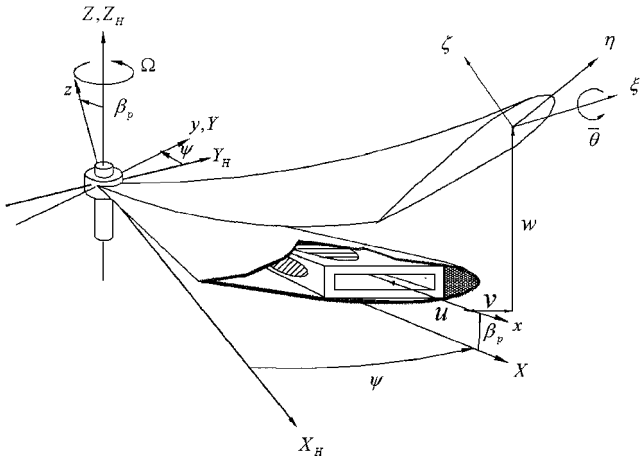

Fig. 1 Geometry and coordinate systems of a blade.

Formulation

Figure 1 shows the schematic of an elastic helicopter blade whose structure is represented as a single-cell, thin-walled laminated composite box beam. Several coordinate systems are used to describe the motion of the blade: the X_H–Y_H–Z_H hub-fixed nonrotating coordinate system, the X–Y–Z hub-rotating coordinate system, the x–y–z undeformed blade coordinate system, and the ξ–η–ζ deformed blade coordinate system. The x–y–z coordinate system is attached to the undeformed blade, which is at a precone angle of β_p in the hub-rotating coordinate system. The deformation of a point on the blade is described by the displacements u, v, w, and ϕ, which are, respectively, axial, chordwise, flatwise, and twist deformations. The chordwise and flatwise displacements, v and w, are expressed as the sum of the displacements due to bending (v_b and w_b) and the displacements due to shear (v_s and w_s) (Ref. 16).

The strain-displacement relations for small strains and moderately large deformations up to second order can be written in the following form:

$$\varepsilon_{xx} = u' + \frac{v_b'^2}{2} + \frac{w_b'^2}{2} - \lambda_T\phi'' + (\eta^2+\zeta^2)\left(\theta_0'\phi' + \frac{\phi'^2}{2}\right) - v_b''(\eta\cos\bar\theta - \zeta\sin\bar\theta) - w_b''(\eta\sin\bar\theta + \zeta\cos\bar\theta)$$

$$\gamma_{x\eta}^t = -\left(\zeta + \frac{\partial\lambda_T}{\partial\eta}\right)\phi', \qquad \gamma_{x\zeta}^t = \left(\eta - \frac{\partial\lambda_T}{\partial\zeta}\right)\phi'$$

$$\gamma_{x\eta}^s = \{v_s'\cos\bar\theta + w_s'\sin\bar\theta\} f_1(\eta,\varsigma)$$

$$\gamma_{x\zeta}^s = \{w_s'\cos\bar\theta - v_s'\sin\bar\theta\} f_2(\eta,\varsigma) \tag{1}$$

where variables with subscript b and s refer to bending and shear deformation, respectively, $\bar\theta = \theta_0 + \phi$ is total geometric pitch of the blade, and λ_T is the St. Venant torsion. Note that, for convenience, the total shear strain components γ_{ij} are divided into two parts: torsion-related strain component γ_{ij}^t and transverse-shear-related strain component γ_{ij}^s. In Eq. (1), f_1 and f_2 denote arbitrary functions in terms of sectional coordinates taking into consideration that the distribution of shear across the cross section is nonuniform (parabolic). As in the theory of a Timoshenko beam, the present approach introduces shear correction coefficients to simplify the analysis. For beams made of composite materials, the shear correction coefficients appear not only to be functions of geometry, but also of the material property of the beam. Kim et al.[19] investigated the distribution of shear for generally orthotropic beams having rectangular solid and thin-walled box sections and formulated the SCF by using the equivalence of shear deformation energies between the real cross section and the equivalent cross section over which the shear stress is uniform. Keeping the aforementioned descriptions in mind, the shear strain components associated with applied tip forces may be written in the following form:

$$\begin{Bmatrix}\bar\gamma_{x\eta}^s\\ \bar\gamma_{x\varsigma}^s\end{Bmatrix} = \begin{bmatrix}1/(k_hGA_h) & 0\\ 0 & 1/(k_vGA_v)\end{bmatrix}\begin{Bmatrix}Q_\eta\\ Q_\varsigma\end{Bmatrix} \tag{2}$$

where the overbar refers to equivalent quantities corresponding to the variables; k_h and k_v are the SCF in edgewise and flatwise directions, respectively; GA_h and GA_v are shear rigidities of the section, respectively; and Q_η and Q_ς are the tip shear forces acting on the blade. Note that, comparing Eqs. (1) and (2), the functions f_1 and f_2 lead to the SCF for the section. For this study, the formula of SCF put forth by Kim et al.[19] has been used (see Appendix).

The constitutive relations of the horizontal and vertical laminas of box-beam walls can be written in the following form:

$$\begin{Bmatrix}\sigma_{xx}\\ \tau_{x\eta}\end{Bmatrix} = \begin{bmatrix}C_{11} & C_{16}\\ C_{16} & C_{66}\end{bmatrix}_h\begin{Bmatrix}\varepsilon_{xx}\\ \gamma_{x\eta}\end{Bmatrix}$$

$$\begin{Bmatrix}\sigma_{xx}\\ \tau_{x\zeta}\end{Bmatrix} = \begin{bmatrix}C_{11} & C_{16}\\ C_{16} & C_{66}\end{bmatrix}_v\begin{Bmatrix}\varepsilon_{xx}\\ \gamma_{x\zeta}\end{Bmatrix} \tag{3}$$

where the subscript h and v denote the horizontal and vertical walls of box section, respectively, and the stiffness coefficients C_{ij} in Eq. (3) are obtained by assuming the state of plane stress in each wall of the box section

$$C_{ij} = \bar Q_{ij} - \bar Q_{i2}\bar Q_{2j}/\bar Q_{22} \qquad \text{for} \qquad i,j = 1,6 \tag{3a}$$

where the expression for the transformed reduced stiffness matrix $\bar Q_{ij}$ in terms of material constants is given by Jones.[24]

The governing differential equations of motion for the composite hingeless rotor can be derived by using the generalized Hamilton's principle in a weak form as

$$\delta\Pi = \int_{t_1}^{t_2}(\delta U - \delta T - \delta W_e)\,\mathrm{d}t = 0 \tag{4}$$

where t_1 and t_2 are arbitrary instants of time and δU, δT, and δW_e are the variation of strain energy, the variation of kinetic energy, and the external virtual work done by external forces, respectively. These are defined as

$$\delta U = \int_0^R\iint_A(\sigma_{xx}\delta\varepsilon_{xx} + \tau_{x\eta}\delta\gamma_{x\eta} + \tau_{x\zeta}\delta\gamma_{x\zeta})\,\mathrm{d}A\,\mathrm{d}x \tag{5}$$

$$\delta T = \int_0^R\iint_A \rho\boldsymbol{V}\cdot\delta\boldsymbol{V}\,\mathrm{d}A\,\mathrm{d}x \tag{6}$$

$$\delta W_e = \int_0^R\Big[L_u\delta u + \big(L_{v_b} + L_{v_s}\big)(\delta v_b + \delta v_s) + \big(L_{w_b} + L_{w_s}\big)(\delta w_b + \delta w_s) + M_\phi\delta p\Big]\,\mathrm{d}x \tag{7}$$

In the kinetic energy expression, Eq. (6), $\boldsymbol{V}$ is the velocity vector of a given point on the deformed elastic axis. On the right-hand side of the virtual work expression, Eq. (7), L_u and M_ϕ are the aerodynamic force and moment distributed along the length of the blade in axial and twist directions, respectively; L_{v_b} and L_{v_s} denote the edgewise components of aerodynamic forces in bending and shear parts, respectively; and L_{w_b} and L_{w_s} denote the flatwise components of aerodynamic forces in bending and shear parts, respectively. In Eq. (7), δp is the virtual rotation of a point along the deformed elastic axis of the blade.[25] The aerodynamic loads acting on the blade are obtained using either quasi-steady or unsteady two-dimensional aerodynamic theory. The effects of compressibility and reversed flow are incorporated in the aerodynamic models. Components of noncirculatory origin aerodynamics are also included. The unsteady aerodynamic model is based on the work of Leishman and Beddoes,[21] and this consists of a linear attached flow solution, a separated flow solution, and a dynamic stall solution. For the present study, only the linear attached unsteady aerodynamics are considered. The linear model uses an indicial response method along with

linear superposition in the form of a finite difference approximation to Duhamel's integral.[21] The Drees linear inflow model (see Ref. 26) is used for the distribution of steady induced inflow.

Note, at this stage, that, because a moderately large deflection for the magnitude of elastic blade motion is assumed in the beam formulation, this study needs a relatively cumbersome mathematical treatment, as well as a tedious process to obtain the final energy expressions in terms of beam displacements and rotations [Eqs. (5–7)]. To save time and labor toward this goal, the present study used a symbolic manipulator such as Mathematica.[27] With special functions provided in the software, the final results, that is, symbolic equations, are directly transformed to the FORTRAN statements, which readily combined into the comprehensive aeroelastic analysis code.

Finite Element Solution Procedure

Applying the finite element method into a discretized form of the Hamilton's principle,[8] one can construct the nonlinear finite element equations of motion in terms of global nodal DOF $\boldsymbol{q}$, which is written in symbolic form as

$$\boldsymbol{M}\ddot{\boldsymbol{q}} + \boldsymbol{C}(\boldsymbol{q}, \psi)\dot{\boldsymbol{q}} + \boldsymbol{K}(\boldsymbol{q}, \psi)\boldsymbol{q} = \boldsymbol{F}(\psi, \boldsymbol{q}, \dot{\boldsymbol{q}}) \tag{8}$$

where $\boldsymbol{M}$, $\boldsymbol{C}$, $\boldsymbol{K}$, and $\boldsymbol{F}$ are the global inertia, damping, stiffness matrices, and load vector, respectively. The damping and stiffness matrices show asymmetry due to the influence of nonconservative aerodynamic forces and moments and are functions of azimuth angle in the rotor disk plane. The blade structure is discretized into a number of beam finite elements. Each beam finite element consists of two end nodes and three internal nodes, which results in a total of 23 DOF per element, including 8 transverse shear DOF, to fully consider the flap–lag–torsion behavior of the blade.[16]

The solution of the governing differential equations of motion (8) requires first the determination of the blade equilibrium position. To reduce computation time required to obtain the steady responses of the blade, the modal superposition technique is applied to the finite element equations. The rotating free vibration analysis is carried out to transform the system mass, damping, and stiffness matrices in the modal space. The resulting transformed modal equations of motion can be written as

$$\bar{\boldsymbol{M}}\ddot{\boldsymbol{r}} + \bar{\boldsymbol{C}}(\psi)\dot{\boldsymbol{r}} + \bar{\boldsymbol{K}}(\boldsymbol{r}, \psi)\boldsymbol{r} = \boldsymbol{Q}_{\mathrm{nl}}(\psi, \boldsymbol{r}, \dot{\boldsymbol{r}}) \tag{9}$$

where $\boldsymbol{r}$ is the generalized modal coordinates and the overbar of the system matrices denotes that the corresponding ones result from modal coordinate transformations. In Eq. (9), all of the nonlinear terms are put in the load vector $\boldsymbol{Q}_{\mathrm{nl}}$ for convenience. The global nodal DOF $\boldsymbol{q}$ can be obtained from the modal coordinates using the transformation as

$$\boldsymbol{q} = \Phi\boldsymbol{r} \tag{10}$$

where Φ is a modal bases matrix that is determined from rotating free vibration analysis. The nonlinear periodic normal mode equations (9) are solved for equilibrium responses using a time finite element technique.[28] The time period of one rotor revolution is discretized into a series of time finite elements, and a periodic boundary condition is imposed by connecting the first and last element.

A coupled trim procedure is used to obtain the nonlinear blade response, pilot control inputs (main rotor collective and cyclic and tail rotor collective), and vehicle orientations (lateral and longitudinal shaft tilt angles) in a simultaneous manner. The coupled trim analysis consists of calculating the vehicle propulsive trim, blade steady deflections, and hub forces and moments. The vehicle propulsive trim involves three force equations (vertical, longitudinal, and lateral) and three moment equations (pitch, roll, and yaw). The propulsive trim solution is used as an initial guess for the blade equilibrium equation and iterated through updating hub forces and moments in the coupled trim algorithm. The nonlinear algebraic equations are solved numerically using the Newton–Raphson technique. The individual contribution of hub forces and moments are obtained using the force summation method, and the multiblade Fourier coordinate transformation (FCT) is applied to convert the rotating blade loads into the fixed frame hub loads. The coupled trim iteration is terminated when the increments of blade steady deflections and propulsive trim variables fall within a given tolerance value.

By the use of the nonlinear deformed position of the blade through the coupled trim analysis, the perturbation eigen analysis is performed to generate the natural modes and to construct the modal flutter equations. For the shaft-fixed stability analysis, the linearized perturbation equations about the equilibrium position are transformed into a first-order form as

$$\begin{Bmatrix} \dot{\tilde{\boldsymbol{p}}} \\ \ddot{\tilde{\boldsymbol{p}}} \end{Bmatrix} = \begin{bmatrix} 0 & \boldsymbol{I} \\ -\bar{\boldsymbol{M}}^{-1}\bar{\boldsymbol{K}}(\boldsymbol{p}_0) & -\bar{\boldsymbol{M}}^{-1}\bar{\boldsymbol{C}}(\boldsymbol{p}_0) \end{bmatrix} \begin{Bmatrix} \tilde{\boldsymbol{p}} \\ \dot{\tilde{\boldsymbol{p}}} \end{Bmatrix} \tag{11}$$

where p_0 is the nonlinear equilibrium position of the blade in modal coordinates and is a function of azimuth angle, and $\tilde{\boldsymbol{p}}$ is the small perturbation about the time-dependent equilibrium position. The transformed modal flutter equations are solved as an algebraic eigenvalue problem with periodic coefficients by using the Floquet transition matrix theory (see Ref. 29), as well as the constant coefficient approximation.[30]

Results and Discussion

The aeroelastic stability analysis of a soft-in-plane composite helicopter blade in forward flight has been performed using the finite element method in space and time. For the present finite element analysis, six spanwise beam finite elements with 23 DOF per element and six time finite elements with a fourth-order interpolation function are used. As a means to save computation time, a modal superposition technique based on rotating vibration modal bases is used for the nonlinear steady response and stability solution. Six normal modes (two flap, two lag, and two torsion) are used for the steady response, and eight normal modes (three flap, two lag, two torsion, one extension) are used for the stability analysis. Note that the elastic coupling results in coupled mode shapes. For convenience, the mode shape that is predominantly bending is referred to as bending mode, and so on. Note also that the quasi-steady aerodynamic theory is used to obtain the aerodynamic loads acting on the blade, except the final unsteady aerodynamics section.

Comparison Study

The current structural dynamics analysis of rotating composite box-beams with bending–torsion and extension–torsion couplings was correlated successfully with other numerical analysis results[14] and experimental test data.[31] The details of the comparison can be found in Ref. 16. To make sure that the current numerical algorithms adopted in the forward flight aeroelastic analysis are properly organized and also to give reliable analysis results, a correlation is conducted with available literature. The work of Smith and Chopra[14] is chosen for this purpose. In Ref. 14, the aeroelastic behavior of a composite hingeless rotor in forward flight was investigated using a refined structural model. A shear flexible 19-DOF beam finite element was developed for the analysis. Figures 2 and 3 show the

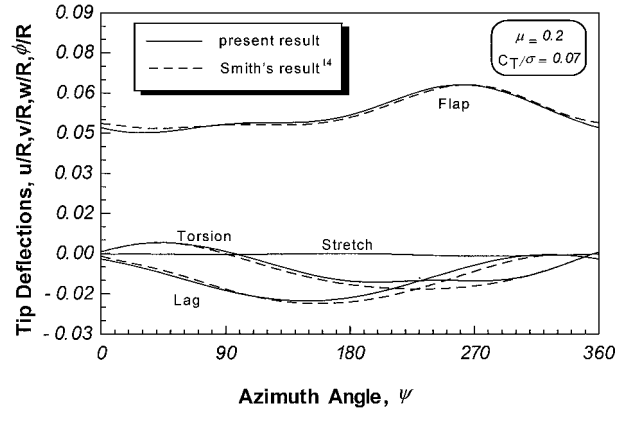

Fig. 2 Comparison of steady tip deflections of a hingeless blade in forward flight ($\mu = 0.2$).

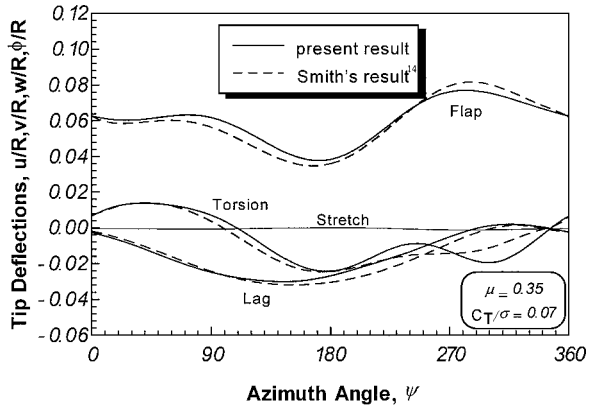

Fig. 3 Comparison of steady tip deflections of a hingeless blade in forward flight ($\mu = 0.35$).

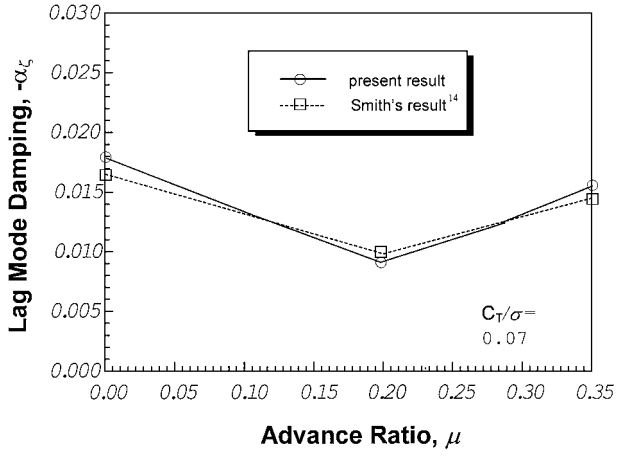

Fig. 4 Comparison of lag mode stability results with forward speed.

comparison results between the two sets of results for steady tip deflections (flap, lag, and torsion) of a soft-in-plane hingeless rotor at an advance ratio of $\mu = 0.2$ and 0.35, respectively. The thrust level is set at $C_T/\sigma = 0.07$. The properties of the vehicle and rotor used in the calculation are similar to those of the production Messerschmitt–Bölkov–Blohm (MBB) BO-105 hingeless rotor design (see Table 2 in Ref. 14). Note that, in Ref. 14, the distribution of shear was assumed (implicitly) to be uniform across the section, and the present results were obtained by using the same assumption for consistency. Fairly good correlation for steady responses at different forward speeds is noticed, as is presented in both Figs. 2 and 3. Figure 4 shows the comparison of the lag mode damping results as a function of forward speed μ. Good correlation is also seen for the stability results at different speeds. Based on the correlation results, the present algorithms and solution schemes employed in the forward flight aeroelastic analysis are thought to be organized well enough for further studies.

Effects of Elastic Couplings

Numerical simulations are conducted to investigate the effects of elastic couplings on the aeroelastic stability of composite hingeless blades. The experimental model rotor of Weller[32] is used for the study. The rotor model has soft-in-plane blade characteristics and is Froude-scaled to simulate overall dynamic properties of production hingeless rotors, with emphasis on the MBB BO-105. The geometric and operational properties of the vehicle and the rotor are summarized in Table 1. The materials used are AS4-3501-6 graphite–epoxy, and the mechanical properties are $E_1 = 141.9$ GPa (20.59×10^6 psi), $E_2 = 9.78$ GPa (1.42×10^6 psi), $G_{12} = 6.0$ GPa (0.87×10^6 psi), and $\nu_{12} = 0.42$. The rotor structure, which is represented as a single-cell box-section beam, is carefully designed to yield realistic values of rotating natural frequencies: fundamental lag frequency $\nu_\zeta = 0.7$, fundamental flap frequency $\nu_\beta = 1.12$, and fundamental torsional frequency $\nu_\phi = 5.0$. The model rotor configurations used in the calculation are divided into seven different cases: baseline uncoupled, pitch–lag coupled (symmetric A and B), pitch–flap coupled (symmetric C and D), and tension–pitch coupled configurations (antisymmetric A and B). Table 2 shows the configuration details of the layup geometry for each of the cases. The positive ply angles are defined as right angles with respect to the beam axis (Fig. 1). The baseline blade consists of a cross-ply layup and, hence, exhibits no elastic couplings. The symmetric case A exhibits positive pitch–lag coupling (lag back/pitch down) and symmetric case C exhibits positive pitch–flap coupling (flap up/pitch down). The antisymmetric case A has positive tension–pitch coupling (tension–pitch down). Each of the other pairs of the layup configurations appeared in Table 2 such as symmetric B, symmetric D, and antisymmetric B presents negative couplings. Table 3 shows the calculation results obtained for rotating flap, lag, and torsion frequencies of the seven cases listed in Table 2. The changes in the frequency values are due to the presence of elastic couplings by the nonzero ply angles in the box-beam walls. The effects are seen to be negligible for the bending modes (within 3%) but substantial for the torsion mode frequencies (maximum 25%). Even though the amplitudes of the torsion mode frequencies for the antisymmetric cases appear a bit higher than those of the conventional ones, the selected cases are thought to fall within the bounds of realistic helicopter blades.

Table 1 Model rotor properties

Parameter	Value
Main rotor	
Number of blades	4
Rotor radius R, in.	52.8
Chord c, in.	3.70
Rotor speed Ω, rpm	660
Lock number γ	6.5
Solidity σ	0.089
Thrust ratio C_T/σ	0.08
Hub length x_{hub}/R	0.015
Precone β_p, deg	−5
Pretwist θ_{tw}, deg	1
Mass per unit length m, slug/ft	0.00866
Vehicle	
Hub vertical offset h/R	0.2
Main rotor c.g. offset x_{cg}/R, y_{cg}/R	0, 0
Flat plate area $f/\pi R^2$	0.01
Tail rotor	
Tail rotor radius r_{tr}/R	0.2
Tail rotor solidity σ_{tr}	0.15
Tail rotor location x_{tr}/R	1.2
Tail rotor above c.g. h_{tr}/R	0.2
Horizontal tail location x_{ht}/R	0.65
Horizon tail planform area $S_{\text{ht}}/\pi R^2$	0.008

Figure 5 shows the stability results for pitch–lag coupled configurations (symmetric cases A and B) as a function of forward speeds. The elastic couplings are seen to play significant roles in the lag mode stability. Compared to the baseline configuration, the negative pitch–lag coupling (symmetric B) has an apparent stabilizing effect on the lag mode, whereas the positive pitch–lag coupling (symmetric A) has a destabilizing effect. The increase in lag mode damping for symmetric case B reaches 170% compared to the baseline case. Note that the stability margin of the symmetric case A improves as the forward speed increases. Results illustrating the effect of nonzero ply angles in the top and bottom walls of the blade structure on the lag mode stability are presented in Fig. 6. It is seen that negative pitch–flap coupling has a stabilizing effect on the lag mode, whereas positive pitch–flap coupling is seen to have a destabilizing effect, though the change of damping appears less substantial than that with pitch–lag couplings. The influence of elastic couplings on the blade stability is demonstrated in a rather dramatic fashion in Fig. 7, where the lag mode damping results for blades with tension–pitch couplings are plotted against the helicopter forward speeds. Positive tension–pitch coupling (antisymmetric A) shows a strong stabilizing effect on the lag mode damping. The increase in lag mode damping for the antisymmetric case A is more than five

Table 2 Configuration of different composite box beams

Case	Top	Bottom	Left	Right
Baseline	$[90/0]_{2s}$	$[90/0]_{2s}$	$[90/0]_{2s}$	$[90/0]_{2s}$
Symmetric A	$[90/0]_{2s}$	$[90/0]_{2s}$	$[30_2/(90/0)_3]$	$[30_2/(90/0)_3]$
Symmetric B	$[90/0]_{2s}$	$[90/0]_{2s}$	$[-30_2/(90/0)_3]$	$[-30_2/(90/0)_3]$
Symmetric C	$[30_2/(90/0)_3]$	$[30_2/(90/0)_3]$	$[90/0]_{2s}$	$[90/0]_{2s}$
Symmetric D	$[-30_2/(90/0)_3]$	$[-30_2/(90/0)_3]$	$[90/0]_{2s}$	$[90/0]_{2s}$
Antisymmetric A	$[-30_2/(90/0)_3]$	$[30_2/(90/0)_3]$	$[-30_2/(90/0)_3]$	$[30_2/(90/0)_3]$
Antisymmetric B	$[30_2/(90/0)_3]$	$[-30_2/(90/0)_3]$	$[30_2/(90/0)_3]$	$[-30_2/(90/0)_3]$

Table 3 Rotating fundamental frequencies at nominal rotor speed ($\Omega = 660$ rpm)

Case	First lag	First flap	First torsion
Baseline	0.721	1.12	5.02
Symmetric A	0.701	1.13	5.32
Symmetric B	0.701	1.13	5.32
Symmetric C	0.720	1.12	5.67
Symmetric D	0.720	1.12	5.67
Antisymmetric A	0.701	1.12	6.28
Antisymmetric B	0.701	1.12	6.28

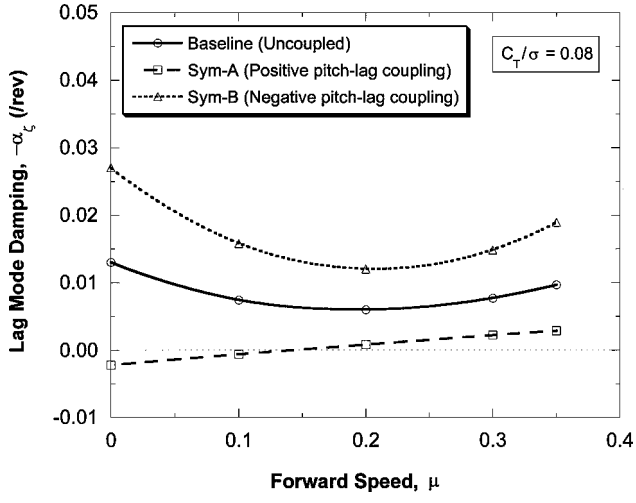

Fig. 5 Lag mode stability results for symmetric A and B with flight speed.

times as much as for the baseline case (maximum 890%), whereas the antisymmetric case B (tension–pitch up coupling) becomes less stable than the baseline case. The increase in lag damping for the case with positive tension–pitch coupling is much larger than that with the negative pitch–lag coupled case (symmetric B).

The preceding results indicate that there is a great potential for the aeroelastic tailoring by using the tension–pitch couplings in the design of a composite blade. Note that this result is consistent with the result obtained for the case 3 configuration in the work of Hong and Chopra[11] and is somewhat different from that of Smith and Chopra,[14] where less significant roles of positive tension–pitch couplings on the lag mode stability were noticed. In Ref. 14, the effects of composite couplings on the aeroelastic stability of composite hingeless rotors in forward flight were investigated. Four specific layup cases representing both positive and negative pitch–flap, negative pitch–lag, and positive tension–pitch couplings, respectively, were considered in the study. Cases with positive pitch–lag and negative tension–pitch couplings were not included in their analysis, whereas, in the present work, all of the configurations (six cases) were considered. In both studies, however, blades with pitch–flap and pitch–lag coupled configurations lead to the same conclusions regarding the blade stability.

Direct Transverse Shear Effects

The influence of transverse shear on the forward flight aeroelastic stability is investigated in this section. The configuration of the blade mentioned in the preceding section is used again for this study.

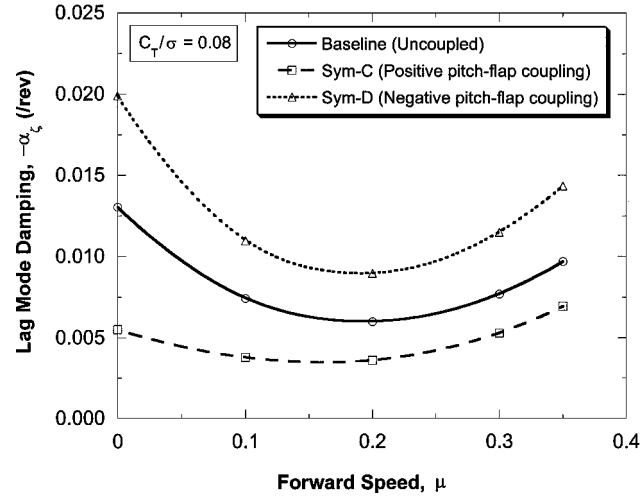

Fig. 6 Lag mode stability results for symmetric C and D with flight speed.

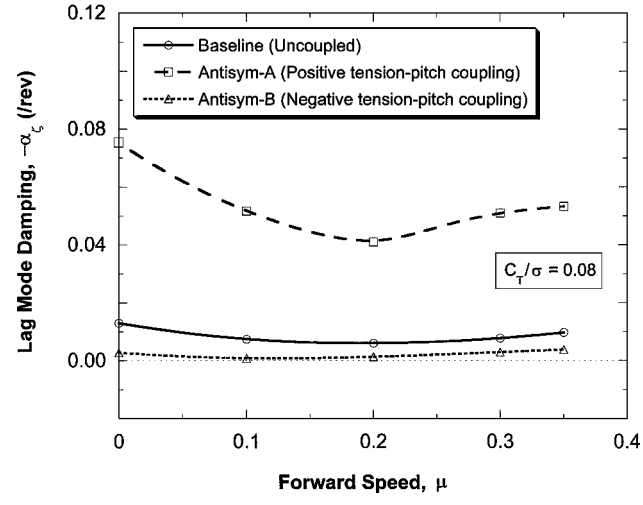

Fig. 7 Lag mode stability results for antisymmetric A and B with flight speed.

Figure 8 shows the effects of transverse shear on the lag mode stability as a function of advance ratios for symmetric cases A and B. It is evident in these pitch–lag coupled cases that, with the introduction of additional flexibility by shear DOF the lag mode becomes more stable than that without considering the shear flexibility. For symmetric case A, the lag mode becomes stable with the introduction of transverse shear, whereas the lag mode remains unstable when the transverse shear is neglected in the analysis. The shear flexibility is believed to play a beneficial role on the stability behavior for this configuration. The stability results with and without considering the shear DOF for baseline and symmetric A cases are presented in Fig. 9. The effects of transverse shear on the lag mode stability present mixed results for these cases: a decrease in lag mode damping for the baseline case and a slight increase in lag mode damping for the symmetric case C. Note that the transverse shear effects

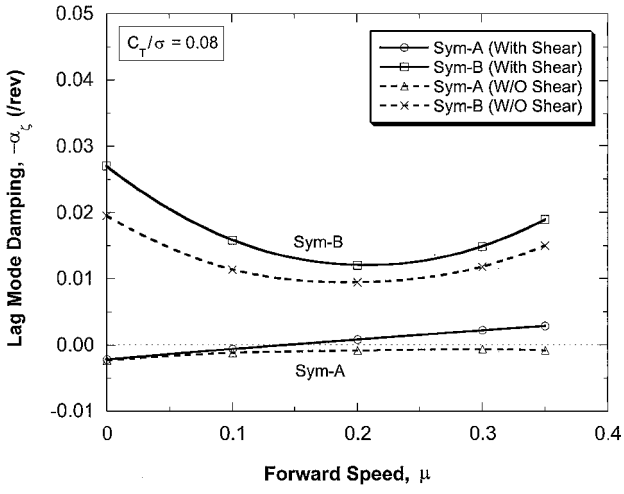

Fig. 8 Effects of transverse shear on lag mode stability for symmetric A and B with flight speeds.

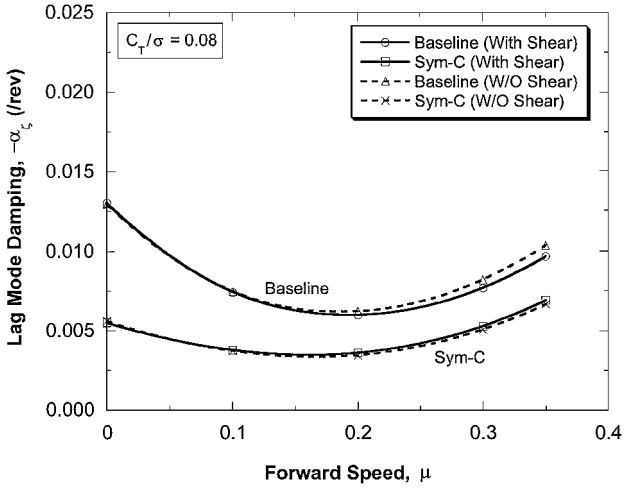

Fig. 9 Effects of transverse shear on lag mode stability for baseline and symmetric C with flight speeds.

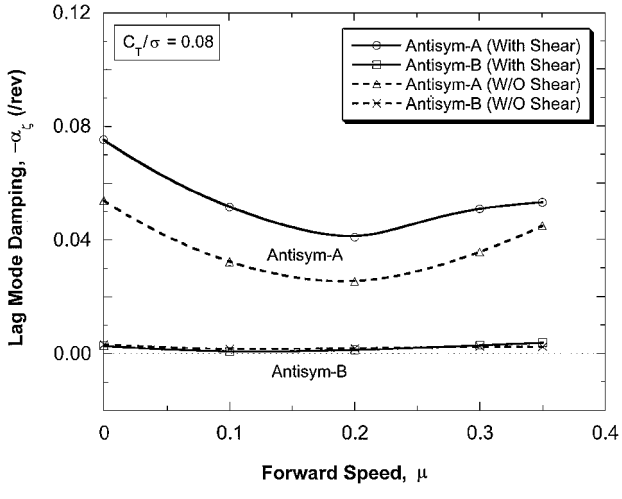

Fig. 10 Effects of transverse shear on the lag mode stability for antisymmetric A and B with flight speeds.

become larger at higher advance ratios as in the cases of symmetric A and B. Figure 10 shows the stability results for antisymmetric cases A and B with and without the transverse shear flexibility. The transverse shear deformation is seen to play a significant role on the lag mode stability for the antisymmetric case A, whereas the effect is negligible for the antisymmetric case B. Note that, overall, the transverse shear flexibility has a stabilizing effect on the lag mode stability for cases with elastic couplings.

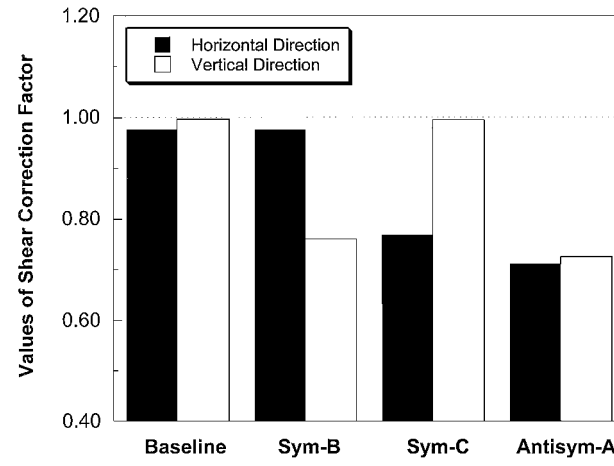

Fig. 11 Shear correction factors in the horizontal and the vertical direction for various configuration blades.

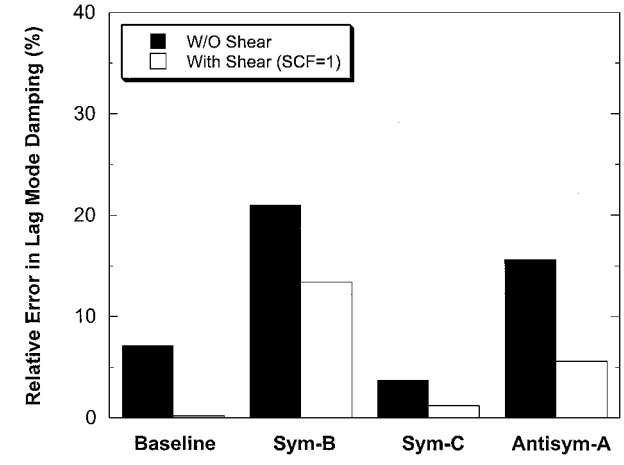

Fig. 12 Effects of transverse shear on the lag mode stability for various configuration blades ($\mu = 0.35$).

In a Timoshenko-like beam theory, the nonuniform distribution of shear across the section of the blade can be taken into account in an effective manner by applying the shear correction factors. For the present study, the formula of SCF put forth by Kim et al.[19] is used to obtain the SCF (see Appendix). The SCF is a function of material properties and layup sequences, as well as the geometry of the section. Calculated results of SCF in the horizontal (chordwise) and vertical (flatwise) directions of the box section for different layup cases are presented in Fig. 11. These values have been used extensively for the blade analysis. Figure 12 shows the relative error in percent in the estimation of the lag mode damping at an advance ratio of $\mu = 0.35$. Results with assuming uniform shear across the section, that is, SCF = 1, and with neglecting transverse shear, are presented together to identify the significance of considering the distribution of shear. The percentage error is defined as $|\alpha_s - \alpha|/\alpha_s \times 100$, where α_s is the damping value with full transverse shear couplings, and α is that without transverse shear or with transverse shear, but with uniform shear. Neglecting transverse shear results in a 3.7–21% error in predicting lag mode damping, whereas assuming uniform shear results in a 0.2–13.4% error.

Unsteady Aerodynamic Effects

Finally, the influence of unsteady aerodynamics on the lag mode stability for a soft-in-plane hingeless rotor is addressed in this section. The vehicle and rotor properties used in the calculation are similar to the full-scale BO-105 hingeless design: rotor radius $R = 193.7$ in., Lock number $\gamma = 7$, solidity $\sigma = 0.089$, and hover tip Mach number $M_{\text{tip}} = 0.7$. For the present study, two different laminate configurations are evaluated: the baseline uncoupled case and

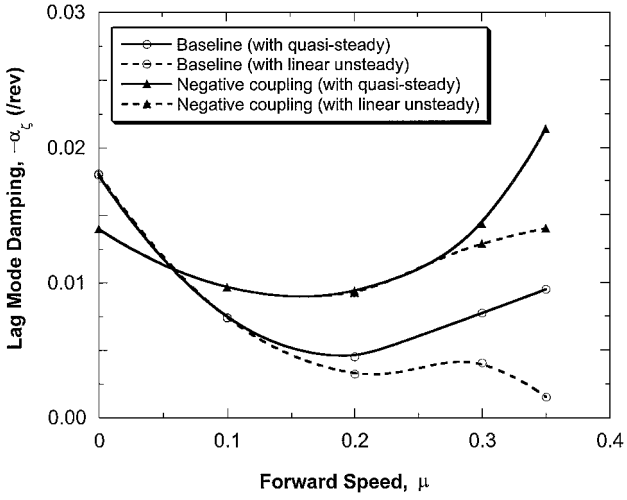

Fig. 13 Effects of unsteady aerodynamics on the lag mode stability for baseline and pitch–lag coupled composite blades with forward speeds.

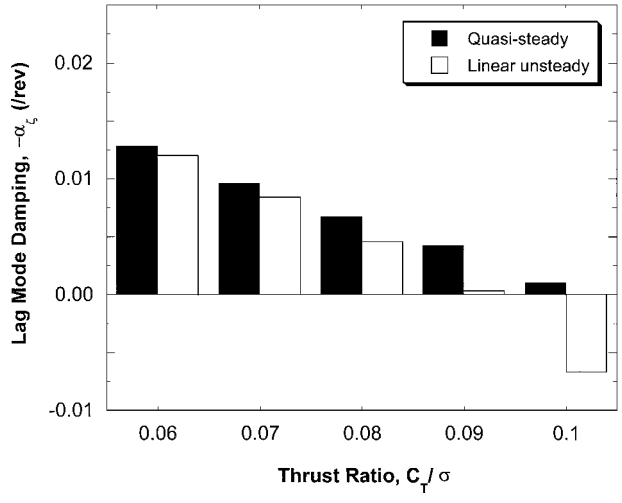

Fig. 14 Effects of unsteady aerodynamics on the lag mode stability for negative pitch–lag coupled composite blades with increasing thrust ratio, $C_T/\sigma(\mu = 0.35)$.

the negative pitch–lag coupled case. The baseline case is composed of $[(90/0)_5/(45/-45)_3/0_4]_s$ so that all of the box-beam walls do not exhibit any elastic couplings. The negative pitch–lag coupled case is composed of $[-30_4/(15/-15)_3/(45/-45)_3/0_4]_s$ for the left and right walls of the box section, whereas the top and bottom walls are composed of $[(90/0)_5/(45/-45)_3/0_4]_s$.

Figure 13 shows the lag mode stability results for both the baseline and negative pitch–lag coupled cases as a function of forward speeds. With the inclusion of negative pitch–lag couplings, a gradual increase of damping with forward speeds is obtained (except near the hover region). It is apparent for both of the configurations that the unsteady effects become dominant at higher forward speeds. With the introduction of unsteady effects, the lag mode damping becomes less stable, especially at very high forward speed ($\mu > 0.3$), than the quasi-steady case. This trend is also clear, as can be seen in Fig. 14, where the thrust level (C_T/σ) of the blade increases from 0.06 to 1.0. At a thrust level of 0.1, the stability result with an unsteady model indicates negative damping, but the case with quasi-steady model shows that the blade still remains in a stable region.

Conclusions

A finite element approach has been performed to investigate the effects of elastic couplings, transverse shear deformation, and unsteady aerodynamics on the aeroelastic stability (shaft-fixed) of composite hingeless rotors in hover and forward flight. In the structural formulation, nonclassical effects such as anisotropy, transverse shear, and torsion warping are incorporated. The nonuniform distribution of shear across a beam section is effectively taken into account by introducing the SCF. The SCF used in this work allows consideration of composite couplings as well as the geometry of the section. The aerodynamic model is formulated to allow either quasi-steady or unsteady two-dimensional aerodynamics. Based on the current work, the following conclusions could be drawn:

1) The present forward flight aeroelastic results for both the steady responses and the stability behavior have been correlated successfully with other literature.

2) Both the negative pitch–lag coupling (lag back/pitch up) and the negative pitch–flap coupling (flap up/pitch up) stabilize the lag motion substantially. This previously known feature of composite couplings is clearly captured through carefully selected blade configurations.

3) An antisymmetric layup blade with positive tension–pitch coupling (tension–pitch down) has a significant stabilizing effect on the lag mode stability and demonstrated a great potential for aeroelastic tailoring: The maximum increase in the lag mode damping reaches 890% compared with the baseline uncoupled blade. On the contrary, the negative tension-pitch coupling has a noticeable destabilizing effect on the blade.

4) The transverse shear deformation presents a definite stabilizing effect on the lag mode stability, especially for cases with elastic couplings. The effects become pronounced at higher forward speeds. Specifically, it is seen in the symmetric A configuration that the lag mode becomes stable with the introduction of transverse shear, whereas the lag mode remains unstable when the transverse shear is neglected in the analysis. The nonuniform distribution of shear should be taken into account appropriately for more accurate results.

5) Inclusion of unsteady aerodynamic effects has substantial influence on the lag mode stability and is important for enhanced aeroelastic analysis. The effects become larger with increasing forward speed and also with increasing thrust ratio.

Appendix: SCF Formula

Figure 1 (also Fig. 3 in Ref. 19) shows the configuration of a thin-walled box-section beam. The box section consists of four walls ($i = 1, 4$), and each wall constitutes local Cartesian system (n_i, s_i) with its origin located at the centroid of each wall. It is assumed that the beam undergoes three degrees of motion: axial displacement u, transverse displacement w, and cross section rotation along the η axis, ψ. The shear correction coefficients are obtained by imposing the equality of shear deformation energies between the actual shear strain and the assumed constant shear strain across the box section, which can be written in a form[19]:

$$\frac{1}{2}\oint N_{xs}\gamma_{xs}a_i^2\,\mathrm{d}s = \frac{1}{2}Q_\zeta(w' - \psi) \tag{A1}$$

where s denotes contour coordinates of the box section; N_{xs} and γ_{xs} are the shear flow and shear strain components along the contour direction, respectively; a_i are the direction sines defined with respect to the horizontal axis; and Q_ζ is the applied tip shear force. Following the procedures described in Ref. 19, the equation for the shear correction coefficient in the vertical direction of the box section is derived as

$$k_\zeta = \frac{Q_\zeta[Q_\zeta - D_{12}u' + D_{23}\psi']}{D_{22}\oint N_{xs}\gamma_{xs}a_i^2\,\mathrm{d}s} \tag{A2}$$

where D_{12}, D_{23}, and D_{22} denote the extension-shear coupling, bending-shear coupling, and direct shear stiffness constants, respectively, and these are defined in Ref. 19. As can be seen in Eq. (A2), the expression for the shear correction coefficient is dependent on material properties, layup sequences, and geometric dimensions of the section. The horizontal counterpart of shear correction coefficient can also be determined in a similar manner.

Acknowledgments

This work was supported by Grant 2001-1-30500-001-2 from the Basic Research Program of the Korea Science and Engineering Foundation. This study has been supported by National Research Laboratory Programs under Contract 00-N-NL-01-C-026.

References

[1]Hodges, D. H., "Review of Composite Rotor Blade Modeling," *AIAA Journal*, Vol. 28, No. 3, 1990, pp. 561–565.

[2]Berdichevsky, V. L., "On the Energy of an Elastic Rod," *PMM*, Vol. 45, No. 4, 1982, pp. 518–529.

[3]Cesnik, C. E. S., and Hodges, D. H., "VABS: A New Concept for Composite Rotor Blade Cross-Sectional Modeling," *Journal of the American Helicopter Society*, Vol. 42, No. 1, 1997, pp. 27–38.

[4]Rehfield, L. W., "Design Analysis Methodology for Composite Rotor Blades," *7th DoD/NASA Conference on Fibrous Composites in Structural Design*, AFWAL-TR-85-3094, Denver, CO, 1985, pp. V(a)1–V(a)5.

[5]Smith, E. C., and Chopra, I., "Formulation and Evaluation of an Analytical Model for Composite Box-Beams," *Journal of the American Helicopter Society*, Vol. 36, No. 3, 1991, pp. 23–35.

[6]Jung, S. N., Nagaraj, V. T., and Chopra, I., "Assessment of Composite Rotor Blade Modeling Techniques," *Journal of the American Helicopter Society*, Vol. 44, No. 3, 1999, pp. 188–205.

[7]Fulton, M. V., and Hodges, D. H., "Aeroelastic Stability of Hingeless, Elastically Tailored Rotor Blades in Hover," *Proceedings of the Winter Annual Meeting of the American Society of Mechanical Engineers*, American Society of Mechanical Engineers, 1992, pp. 9–23.

[8]Shang, X., Hodges, D. H., and Peters, D. A., "Aeroelastic Stability of Composite Hingeless Rotors in Hover with Finite-State Unsteady Aerodynamics,"*Journal of the American Helicopter Society*, Vol. 44, No. 3, 1999, pp. 206–221.

[9]Sharpe, D. L., "An Experimental Investigation of the Flap-Lag-Torsion Aeroelastic Stability of a Small-Scale Hingeless Helicopter Rotor in Hover," NASA TP 2546, Jan. 1986.

[10]Friedmann, P. P., "Helicopter Rotor Dynamics and Aeroelasticity: Some Key Ideas and Insights," *Vertica*, Vol. 14, No. 1, 1990, pp. 101–121.

[11]Hong, C. H., and Chopra, I., "Aeroelastic Stability Analysis of a Composite Rotor Blade," *Journal of the American Helicopter Society*, Vol. 30, No. 2, 1985, pp. 57–67.

[12]Panda, B., and Chopra, I., "Dynamics of Composite Rotor Blades in Forward Flight," *Vertica*, Vol. 11, No. 1/2, 1987, pp. 107–209.

[13]Yuan, K. A., Friedmann, P. P., and Venkatesan, C., "Aeroelastic Behavior of Composite Rotor Blades with Swept Tips," *48th Annual Forum of the American Helicopter Society*, American Helicopter Society, Alexandria, VA, 1992, pp. 1039–1059.

[14]Smith, E. C., and Chopra, I., "Aeroelastic Response and Blade Loads of a Composite Rotor in Forward Flight," *Proceedings of the 33rd Structures, Structural Dynamics, and Materials Conference*, AIAA, Washington, DC, 1992, pp. 1996–2014.

[15]Tracy, A. L., and Chopra, I., "Aeroelastic Analysis of a Composite Bearingless Rotor in Forward Flight Using an Improved Warping Model," *Journal of the American Helicopter Society*, Vol. 40, No. 3, 1995, pp. 80–91.

[16]Jung, S. N., and Kim, S. J., "Aeroelastic Response of Composite Rotor Blades Considering Transverse Shear and Structural Damping," *AIAA Journal*, Vol. 32, No. 4, 1994, pp. 820–827.

[17]Jung, S. N., and Kim, S. J., "Effect of Transverse Shear on Aeroelastic Stability of a Composite Rotor Blade," *AIAA Journal*, Vol. 33, No. 8, 1995, pp. 1541–1543.

[18]Cowper, G. R., "The Shear Coefficient in Timoshenko's Beam Theory," *Journal of Applied Mechanics*, Vol. 33, 1966, pp. 335–340.

[19]Kim, S. J., Yoon, K W., and Jung, S. N., "Shear Correction Factors for Thin-Walled Composite Boxbeam Considering Nonclassical Behaviors," *Journal of Composite Materials*, Vol. 30, No. 10, 1996, pp. 1133–1149.

[20]Rehfield, L. W., Atilgan, A. R., and Hodges, D. H., "Nonclassical Behavior of Thin-Walled Composite Beams with Closed Cross Sections," *Journal of the American Helicopter Society*, Vol. 35, No. 2, 1990, pp. 42–50.

[21]Leishman, J. G., and Beddoes, T. S., "A Semi-Empirical Model for Dynamic Stall," *Journal of the American Helicopter Society*, Vol. 34, No. 3, 1989, pp. 3–17.

[22]Volovoi, V. V., and Hodges, D. H., "Theory of Anisotropic Thin-Walled Beams," *Journal of Applied Mechanics*, Vol. 67, No. 3, 2000, pp. 453–459.

[23]Jung, S. N., Nagaraj, V. T., and Chopra, I., "Refined Structural Model for Thin- and Thick-Walled Composite Rotor Blades," *AIAA Journal*, Vol. 40, No. 1, 2002, pp. 105–116.

[24]Jones, R. M., *Mechanics of Composite Materials*, McGraw–Hill, New York, 1975, pp. 45–51.

[25]Hodges, D. H., Ormiston, R. A., and Peters, D. A., "On the Nonlinear Deformation Geometry of Euler–Bernoulli Beams," NASA TP 1566, April 1980.

[26]Panda, B., and Chopra, I., "Flap-Lag-Torsion Stability in Forward Flight," *Journal of the American Helicopter Society*, Vol. 30, No. 4, 1985, pp. 30–39.

[27]Wolfram, S., *Mathmatica: A System for Doing Mathematics by Computer*, Addison Wesley Longman, Reading, MA, 1991, pp. 87–104.

[28]Borri, M., "Helicopter Rotor Dynamics by Finite Element Time Approximation," *Computers and Mathematics with Applications*, Vol. 12A, No. 1, 1986, pp.149–160.

[29]Dugundji, J., and Wendell, J. H., "Some Analysis Methods for Rotating Systems with Periodic Coefficients," *AIAA Journal*, Vol. 21, No. 6, 1983, pp. 890–897.

[30]Johnson, W., *Helicopter Theory*, Princeton Univ. Press, Princeton, NJ, 1980, Chap. 11.

[31]Chandra, R., and Chopra, I., "Experimental-Theoretical-Investigation of the Vibration Characteristics of Rotating Composite Box Beams," *Journal of Aircraft*, Vol. 29, No. 4, 1992, pp. 657–664.

[32]Weller, W. H., "Relative Aeromechanical Stability Characteristics for Hingeless and Bearingless Rotors," *Journal of the American Helicopter Society*, Vol. 35, No. 3, 1990, pp. 68–77.

E. Livne
Associate Editor